IEEE Transactions on Automation Science and Engineering (T-ASE) paper, presented at ICRA 2024, Yokohama, Japan. Cite as T-ASE paper.

A Hybrid Controller Enhancing Transient Performance for an Aerial Manipulator Extracting a Wedged Object

Jeonghyun Byun, *Graduate Student Member, IEEE*, Inkyu Jang, *Graduate Student Member, IEEE*, Dongjae Lee, *Graduate Student Member, IEEE*, and H. Jin Kim, *Member, IEEE*

***Abstract*— Autonomous aerial manipulation requires the capability to handle inevitable dynamic changes during physical interaction. Previously, very few studies have addressed the stability and transient performance of the scenarios involving abrupt changes in dynamics. This paper proposes a hybrid controller enhancing transient performance for an aerial manipulator extracting an object wedged in a static structure. This task incurs a significant jump in the interaction force on the end-effector so that the analysis using the concept of hybrid dynamical systems is required. To demonstrate the dynamic characteristics of the object-extracting aerial manipulator, we derive the dynamic equations for two flight modes, i.e., free-flight and object-extracting, and the rule of state jumps. Also, we design control strategies which enhance the transient performance during flight mode transition. Then, the stability of the proposed control law is proven, and the overshoot reduction after the object extraction is analyzed. To show the improved performance, we conduct plug-pulling experiments with a quadrotor-based aerial manipulator using the proposed controller and two different existing controllers. The comparative results confirm that our controller enables the aerial manipulator to maintain its stability after the flight mode transition and shows the best transient performance in overshoot minimization among three controllers.**

***Note to Practitioners*—The motivation for this article is the desire to prevent unexpected collisions between obstacles and an aerial manipulator after the vehicle extracts a wedged object from a static structure. To resolve this problem, we present a hybrid control method for such tasks while avoiding an excessive overshoot after the extraction. This method can be utilized in tasks involving abrupt changes in the dynamic model such as retrieving a device attached to a tall structure, reclaiming an object in disaster recovery, or pulling a plug out of a socket. Unlike existing methods, the proposed method simultaneously considers the stability *and* the initial overshoot right after pulling the object out of the structure, by employing a disturbance observer (DOB) in a hybrid control structure. It can be utilized for the aerial manipulator to avoid collision in a narrow space or to keep it in a safe operation envelope even though the task requires producing a relatively large pulling force.**

***Index Terms*— Hybrid control, transient performance analysis, disturbance observer (DOB), aerial manipulator.**

Manuscript received 5 April 2023; accepted 11 May 2023. This article was recommended for publication by Associate Editor Z. Pei and Editor M. Dotoli upon evaluation of the reviewers' comments. This work was supported in part by the Unmanned Vehicles Core Technology Research and Development Program through the National Research Foundation of Korea (NRF); and in part by the Unmanned Vehicle Advanced Research Center (UVARC) funded by the Ministry of Science and Information and Communication Technology (ICT), Republic of Korea, under Grant NRF-2020M3C1C1A01086411. *(Corresponding author: H. Jin Kim.)*

Jeonghyun Byun and H. Jin Kim are with the Department of Aerospace Engineering, Automation and System Research Institute (ASRI), and the Institute of Advanced Aerospace Technology (IAAT), Seoul National University, Seoul 08826, South Korea (e-mail: quswjdgus97@snu.ac.kr; hjinkim@snu.ac.kr).

Inkyu Jang is with the Department of Aerospace Engineering and the Automation and System Research Institute (ASRI), Seoul National University, Seoul 08826, South Korea (e-mail: leplusbon@snu.ac.kr).

Dongjae Lee is with the Department of Aerospace Engineering and the Institute of Advanced Aerospace Technology (IAAT), Seoul National University, Seoul 08826, South Korea (e-mail: ehdwo713@snu.ac.kr).

This article has supplementary material provided by the authors and color versions of one or more figures available at https://doi.org/10.1109/TASE.2023.3277508.

Digital Object Identifier 10.1109/TASE.2023.3277508

I. Introduction

AERIAL manipulation has been gaining a powerful appeal in research and industry thanks to the combination of the maneuverability of an unmanned aerial vehicle (UAV) and the versatility of a robotic manipulator. Heretofore, there had been several research on control of aerial manipulation tasks such as valve turning [1], drawer opening [2], door opening [3], or window-cleaning robot installation [4]. However, most of them only considered a single dynamic model to construct the control laws.

Since an aerial manipulator conducting a physically interacting task undergoes at least two flight modes including free-flight and task-operating, there needs a controller that can deal with dynamic model changes during flight mode transition. Especially, there are various operations that necessarily entail an abrupt change in dynamic model, e.g., the disappearance of a pulling force while extracting an object wedged or stuck in a static structure, or the sudden increase of speed when the type of friction force changes while pushing a movable structure.

Among such tasks, this paper treats the problem of extracting an object wedged in a static structure since this task has several real-world applications such as retrieving a device attached to a tall structure, or reclaiming an object in disaster recovery mission. As a laboratory-scale example of a similar situation, we conduct a plug-pulling experiment. There exist very few studies on control of an aerial manipulator under an abrupt dynamic model change [6], [7]. Furthermore, they did not simultaneously consider the overall stability and transient performance after flight mode transition. Therefore, there needs a new control strategy to extract the object with a mitigated overshoot in a state variable.

IEEE Transactions on Automation Science and Engineering (T-ASE) paper, presented at ICRA 2024, Yokohama, Japan.

A. Related Works

Most studies on aerial manipulator control utilized adaptive or robust controllers to deal with dynamic model changes caused by flight mode transition. References [8], [9], [10], and [11] presented adaptive controllers which guarantee the stability under the condition that disturbance and its time-derivative are bounded. In [7] and [12], robust controllers which keep the aerial manipulator stable under the same conditions are introduced. However, they are not suitable for the object-extracting task during which the time-derivative of the disturbance may become unbounded due to the sudden disappearance of a pulling force. In [13], gain-scheduling was utilized to adapt to the change in dynamic model. However, since it takes time for the controller gains to become adjusted to suitable values for stabilization in the changed flight mode, an excessive overshoot in the state variable may occur during such time.

To resolve the above problems, several studies dealt with UAVs that follow two or more flight modes. In [14] and [15], a switching motion/force controller was designed for a UAV that makes contact with its surroundings. Reference [16] designed a hybrid controller for a flying-walking robot which has two modes of flying and walking. However, these works did not analyze the stability during the mode change. Also, [17] created a new aerial platform which can pass through a narrow gap and apply strong force to the surrounding environment, and separated its dynamic model into three flight modes. However, the stability during the flight mode transition was not rigorously investigated.

Only a few studies analyzed stability during flight mode transition. References [18] and [19] proposed the control methods for a UAV that physically interacts with its surroundings and proved the stability of the vehicle between free and contact motion. Reference [20] divided the process of a UAV landing on a slope into several flight modes and proved the stability of the entire process. However, since the effect of dynamic model change can be mitigated by slowing down before the physical contact for the tasks such as approaching a wall or a landing site, such strategy may not suffice to guarantee the stability of the tasks involving an abrupt change in dynamic model.

Our previous work [6] designed a hybrid DOB (Disturbance OBserver)-based controller for an aerial manipulator conducting a plug-pulling task which is one of the object-extracting tasks. However, there was no explicit consideration on the initial overshoot in the state variable that occurs after the plug separation.

B. Contributions

In this paper, we propose a hybrid controller enhancing transient performance for an aerial manipulator extracting a wedged object from a static structure. Control strategies enhancing the transient performance during flight mode transition are designed for each flight mode, and we theoretically prove that the magnitude of the initial overshoot in the state variable right after the object extraction is bounded. As an example of such task, we conduct a plug-pulling experiment,

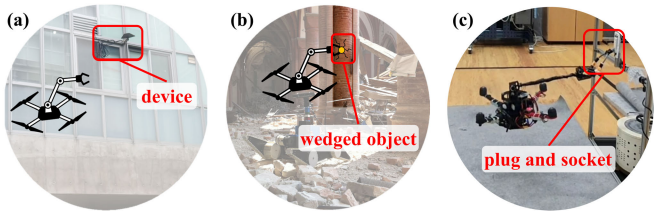

Fig. 1. Examples of extracting an object wedged in a static structure. (a) Retrieving a device attached to a tall structure, (b) reclaiming an object in disaster recovery mission [5] and (c) pulling a plug out of a socket [6].

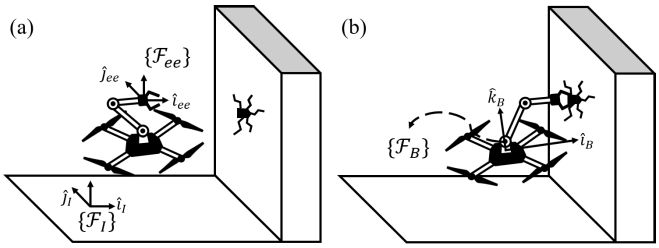

Fig. 2. (a) Free-flight (F) and (b) Object-extracting (E) modes of the aerial manipulator extracting an object wedged in a static structure with the coordinate frames.

and the results of using the proposed controller are compared with those of using two different existing control methods.

C. Outline

In Section II, we formulate two dynamic equations of the aerial manipulator corresponding to the two flight modes, i.e., free flight and object-extracting, and we describe the hybrid controller enhancing transient performance in Section III. In Section IV, we present the analyses on the stability and the transient performance after the flight mode transition, and the proposed controllers are validated experimentally in Section V, where the experimental setup and results are reported.

Notations: 0_{ij}, I_i and e_3 represent the $i \times j$ zero matrix, $i \times i$ identity matrix and $[0\ 0\ 1]^\top$, respectively. $|\alpha|$ and α_i mean the Euclidean norm and the i-th element of a vector α, respectively. Also, given two matrices A and B, $\|A\|$ represents the 2-norm of A and $A \otimes B$ means the Kronecker product of A and B. The operator $S(\cdot)$ maps a vector into a skew-symmetric matrix such as $S(\alpha)\beta = \alpha \times \beta$ for two vectors α and β. Furthermore, c_* and s_* are the abbreviations of $\cos *$ and $\sin *$, respectively.

II. Dynamic Models of the Aerial Manipulator

The aerial manipulator conducting an object-extracting task is described by two flight modes: free-flight (F) and object-extracting (E). As shown in Figure 2, the F mode describes the aerial manipulator flying in the free space while the E mode expresses the aerial manipulator holding onto the wedged object.

In Figure 2, each dynamic model is constructed with the following coordinate frames: the inertial frame $\{\mathcal{F}_I\}$, the multi-rotor frame $\{\mathcal{F}_B\}$, the i-th added object frame $\{\mathcal{F}_i\}$ ($i \in \{1, \cdots, n\}$), and the end-effector frame $\{\mathcal{F}_{ee}\}$. The position and attitude of $\{\mathcal{F}_B\}$ with respect to $\{\mathcal{F}_I\}$ are $p_B \triangleq [p_x\ p_y\ p_z]^\top$ and $\phi \triangleq [\phi_x\ \phi_y\ \phi_z]^\top$, respectively, where ϕ follows the ZYX Euler angle convention. The generalized

IEEE Transactions on Automation Science and Engineering (T-ASE) paper, presented at ICRA 2024, Yokohama, Japan.

coordinate of the multi-rotor is defined as $\chi \triangleq [p_B^\top \ \phi^\top]^\top$, and the control input to the multi-rotor is $u \triangleq [T \ \tau_B]$ where T and τ_B represent the total thrust and the body torque, respectively.

A. Free-Flight (F) Mode

The dynamic equation of the aerial manipulator in the F mode is expressed as follows [21]:

$$M\ddot{\chi} + C\dot{\chi} + K = \hat{Q}^\top u + \delta_\chi \tag{1}$$

where $M \in \mathbb{R}^{6\times6}$, $C \in \mathbb{R}^{6\times6}$, and $K \in \mathbb{R}^6$ represent the inertia matrix, Coriolis-centrifugal terms, and gravity effects, respectively. Also, the input matrix $\hat{Q}$ and the mapping matrix Q are formulated as follows:

$$\omega_B^B = Q\dot{\phi}, \quad \hat{Q} \triangleq \begin{bmatrix} e_3^\top R_B^\top & 0_{13} \\ 0_{33} & Q \end{bmatrix}$$

where $R_B \in SO(3)$ denotes the rotation matrix from $\{\mathcal{F}_B\}$ to $\{\mathcal{F}_I\}$, and ω_B^B means the angular velocity of $\{\mathcal{F}_B\}$ with respect to $\{\mathcal{F}_I\}$ expressed in $\{\mathcal{F}_B\}$. Moreover, δ_χ represents the lumped disturbance term which includes the external wrenches exerted on the aerial manipulator and the dynamic effect caused by the motion of the n added objects [21].

Since the dimension of the control input u is smaller than that of the generalized coordinate χ, the aerial manipulator is an underactuated system. Thus, (1) is expressed as a cascaded system composed of two subsystems: underactuated and fully actuated.

1) Underactuated Subsystem: The underactuated subsystem of the F mode is arranged as follows [22]:

$$\ddot{z}_\mathrm{u} = G_\mathrm{u}\Phi_d + \Delta_\mathrm{u,F} \tag{2}$$

where z_u represents the x and y coordinates of the aerial manipulator's center of mass while the desired value of Φ, Φ_d, acts as a control input. Also,

$$G_\mathrm{u} \triangleq \frac{T}{m_t}\begin{bmatrix} c_{\phi_z} & s_{\phi_z} \\ s_{\phi_z} & -c_{\phi_z} \end{bmatrix}, \quad \Phi \triangleq \begin{bmatrix} c_{\phi_x} s_{\phi_y} \\ s_{\phi_x} \end{bmatrix},$$
$$\Delta_\mathrm{u,F} \triangleq G_\mathrm{u}(\Phi - \Phi_d) + \frac{1}{m_t}[I_2 \ 0_{24}]\delta_\chi$$

with the total mass of the aerial manipulator m_t.

2) Fully Actuated Subsystem: By multiplying $[0_{24} \ I_4]M^{-1}$ into (1), the fully actuated subsystem of the F mode is obtained as follows:

$$\ddot{z}_\mathrm{f} = F_\mathrm{f} + G_\mathrm{f}u + \Delta_\mathrm{f,F} \tag{3}$$

where $z_\mathrm{f} \triangleq [p_z \ \phi^\top]^\top$, $F_\mathrm{f} \triangleq [0_{42} \ I_4]M^{-1}(-C\dot{\chi} - K)$, $G_\mathrm{f} \triangleq [0_{42} \ I_4] \ M^{-1}\hat{Q}^\top[0_{42} \ I_4]^\top$, and $\Delta_\mathrm{f,F} \triangleq [0_{42} \ I_4] \ M^{-1}\delta_\chi$.

B. Object-Extracting (E) Mode

For the aerial manipulator in the E mode, the position of the end-effector is almost constant so that the velocity of the end-effector with respect to $\{\mathcal{F}_I\}$, $\dot{p}_{ee} = J_{ee}(\chi)\dot{\chi}$, is approximately zero and the small movement, which occurs due to the loose grabbing of the wedged object, is lumped into δ_χ. Therefore, the Lagrange-Euler equation with the kinematic constraint is derived as follows:

$$M\ddot{\chi} + C\dot{\chi} + K = \hat{Q}^\top u + J_{ee}^\top(\chi)F_{ee} + \delta_\chi \tag{4}$$

where

$$J_{ee}(\chi) \triangleq \frac{\partial p_{ee}}{\partial \chi} = [I_3 \ -S(R_B p_{Bee})Q]$$
$$F_{ee} \triangleq (J_{ee}M^{-1}J_{ee}^\top)^{-1} \times \{-\dot{J}_{ee}\dot{\chi} + J_{ee}M^{-1}(\hat{Q}^\top u - C\dot{\chi} - K)\}$$

where p_{Bee} represents the position of the end-effector with respect to $\{\mathcal{F}_B\}$.

As in (2) and (3), we also decouple (4) into the underactuated and fully actuated subsystems as follows:

$$\ddot{z}_\mathrm{u} = G_\mathrm{u}\Phi_d + \Delta_\mathrm{u,E} \tag{5}$$
$$\ddot{z}_\mathrm{f} = F_\mathrm{f} + G_\mathrm{f}u + \Delta_\mathrm{f,E} \tag{6}$$

where $\Delta_\mathrm{u,E} \triangleq G_\mathrm{u}(\Phi - \Phi_d) + \frac{1}{m_t}[I_2 \ 0_{24}](J_{ee}^\top F_{ee} + \delta_\chi)$ and $\Delta_\mathrm{f,E} \triangleq [0_{42} \ I_4]M^{-1}(J_{ee}^\top F_{ee} + \delta_\chi)$.

C. Jump Map

According to [23], the jump map represents the change of states after the flight mode transition. Since the aerial manipulator does not collide with the surrounding environment during the task operation, $[\chi \ \dot{\chi}]^\top$ does not change after the flight mode transition. Meanwhile, since the force exerted on the end-effector, F_{ee} in (4), abruptly occurs when the flight mode is changed from free-flight (F) to object-extracting (E), and suddenly vanishes when the flight mode change occurs in the opposite direction, $\ddot{\chi}$ undergoes the jump in its value. Thus, the jump maps for χ, $\dot{\chi}$ and $\ddot{\chi}$ are expressed as follows:

$$\begin{aligned} \chi^+ &= \chi, \\ \dot{\chi}^+ &= \dot{\chi}, \\ \ddot{\chi}^+ &= \begin{cases} \ddot{\chi} + M^{-1}J_{ee}^\top F_{ee}, & \text{if F} \longrightarrow \text{E} \\ \ddot{\chi} - M^{-1}J_{ee}^\top F_{ee}, & \text{else,} \end{cases} \end{aligned} \tag{7}$$

where the superscript $+$ means the value immediately after the flight mode transition.

D. Nominal Models

Since DOBs are designed for each subsystem, the nominal models for the respective subsystems are required. For the underactuated subsystem, since the dynamic equations (2) and (5) are expressed in the same structure as $\ddot{z}_\mathrm{u} = G_\mathrm{u}\Phi_d + \Delta_{\mathrm{u},\mu}$ where $\mu \in \{\mathrm{F}, \mathrm{E}\}$, we utilize the same nominal model for each flight mode. Similarly, since (3) and (6) are expressed in $\ddot{z}_\mathrm{f} = F_\mathrm{f} + G_\mathrm{f}u + \Delta_{\mathrm{f},\mu}$, we also utilized the same nominal model of the fully actuated subsystem for both flight modes.

1) Underactuated Subsystem: The nominal model is formulated as follows:

$$\ddot{z}_\mathrm{u} = \bar{G}_\mathrm{u}\bar{\Phi}_d \tag{8}$$

where

$$\bar{G}_\mathrm{u} \triangleq \frac{\bar{T}}{\bar{m}_t}\begin{bmatrix} c_{\phi_z} & s_{\phi_z} \\ -s_{\phi_z} & c_{\phi_z} \end{bmatrix}$$

and $\bar{\Phi}_d$ means the nominal value of Φ_d with the measured value of m_t, $\bar{m}_t$. Also, we let $\bar{T}$ denote the value of the total thrust generated from our control law, while T represents the thrust produced by the rotation of the propellers.

IEEE Transactions on Automation Science and Engineering (T-ASE) paper, presented at ICRA 2024, Yokohama, Japan.

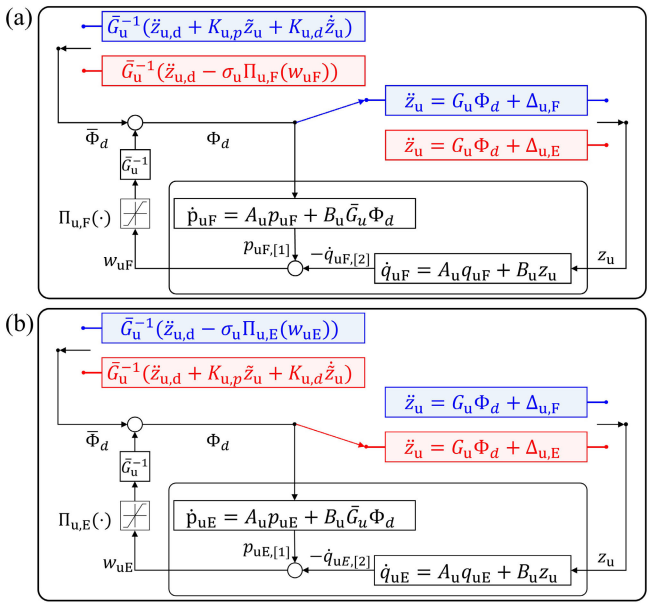

Fig. 3. Update laws for the underactuated subsystem's inner-DOB variables (a) (p_{uF}, q_{uF}) and (b) (p_{uE}, q_{uE}). Blue and red shaded regions are activated during the F and E modes, respectively.

2) Fully Actuated Subsystem [21]: The nominal model is arranged as follows:

$$\ddot{z}_f = \bar{F}_f + \bar{G}_f \bar{u} \tag{9}$$

where $\bar{u}$ represents the nominal value of u. Also,

$$\bar{G}_f \triangleq \begin{bmatrix} \frac{c_{\phi_x} c_{\phi_y}}{\bar{m}_B} & 0_{13} \\ 0_{31} & Q^{-1}\bar{J}_B \end{bmatrix},$$
$$\bar{F}_f \triangleq \begin{bmatrix} -\bar{g} \\ -Q^{-1}\{\dot{Q}\dot{\phi} + \bar{J}_B^{-1} S(\omega_B^B)\bar{J}_B \omega_B^B\} \end{bmatrix}$$

where $\bar{g}$, $\bar{m}_B$ and $\bar{J}_B$ mean the nominal values of the gravitational acceleration g, the mass of the multi-rotor m_B and the moment of inertia of the multi-rotor J_B, respectively.

III. Hybrid Controller Enhancing Transient Performance

In this section, we first divide the controller structure into two subsystems: underactuated and fully actuated. For each subsystem, additional strategies to enhance the transient performance immediately after the flight mode transition are designed while the control laws are identical for both modes.

Throughout the controller designs, we let α_d denote the desired value of a vector α. Also, for a vector β with $2N$ elements with $N \in \mathbb{N}$, $\beta_{[1]}$ and $\beta_{[2]}$ represent $[\beta_1 \ \cdots \ \beta_{2N-1}]^\top$ and $[\beta_2 \ \cdots \ \beta_{2N}]^\top$, respectively.

A. Underactuated Subsystem

For each flight mode, Φ_d is calculated by the DOB-based control law introduced in [7]. Even though the structures of the DOBs are the same in both F and E modes, we use different inner variables for two flight modes to separately operate the respective DOBs: q_{uF}, $p_{uF} \in \mathbb{R}^4$ for the F mode and q_{uE}, $p_{uE} \in \mathbb{R}^4$ for the E mode. Also, to avoid the undesirable peaking in Φ_d, we utilize the saturation functions $\Pi_{u,F}(\cdot)$ and $\Pi_{u,E}(\cdot)$ defined as follows:

- $\Pi_{u,\mu}(\cdot)$: $\mathbb{R}^2 \to \mathbb{R}^2$ is a globally bounded $\mathcal{C}^1$ function,
- $\Pi_{u,\mu}(w) = w, \ \forall w \in S_{u,\mu} \triangleq \{w \in \mathbb{R}^2 \mid w = \bar{G}_u G_u^{-1}((\bar{G}_u - G_u)\bar{\Phi}_d - \Delta_{u,\mu})\}$,
- $\|\partial \Pi_{u,\mu}(w)/\partial w\| \le 1$

with $\mu \in \{F, E\}$. Then, from the calculated Φ_d, the desired roll and pitch angles are obtained as follows:

$$\phi_{x,d} = \sin^{-1}(\Phi_{d,2}), \quad \phi_{y,d} = \sin^{-1}(\Phi_{d,1}/c_{\phi_{x,d}}). \tag{10}$$

In the following sections, the DOB-based control laws and the strategies to enhance the transient performance will be presented for each flight mode.

1) Free-Flight (F) Mode: First, we set $\bar{\Phi}_d$ as a PD control

$$\bar{\Phi}_d = \bar{G}_u^{-1}(\ddot{z}_{u,d} + K_{u,P}\tilde{z}_u + K_{u,D}\dot{\tilde{z}}_u) \tag{11}$$

to make the nominal model (8) asymptotically stable. Using this value, to compensate for the model uncertainty between the actual model (2) and the nominal model (8), the DOB-based control law is formulated as follows:

$$\begin{aligned} \dot{q}_{uF} &= A_u q_{uF} + B_u z_u, \quad \dot{p}_{uF} = A_u p_{uF} + B_u \bar{G}_u \bar{\Phi}_d \\ w_{uF} &= p_{uF,[1]} - \dot{q}_{uF,[2]}, \quad \Phi_d = \bar{\Phi}_d + \bar{G}_u^{-1}\Pi_{u,F}(w_{uF}) \end{aligned} \tag{12}$$

where

$$A_u \triangleq I_2 \otimes \begin{bmatrix} 0 & 1 \\ -a_{u0}/\epsilon_u^2 & -a_{u1}/\epsilon_u \end{bmatrix},$$
$$B_u \triangleq I_2 \otimes [0 \quad a_{u1}/\epsilon_u^2]^\top$$

with the positive parameters a_{u0}, a_{u1} and ϵ_u which satisfy $a_{u0}^2/a_{u1} < \frac{1}{2}$ and $\epsilon_u \ll 1$.

If we substitute Φ_d in (12) for (2), the dynamic equation is rearranged as follows:

$$\ddot{z}_u = \underbrace{\bar{G}_u\bar{\Phi}_d}_{\text{nominal part}} + \underbrace{(G_u - \bar{G}_u)\bar{\Phi}_d + \Delta_{u,F}}_{\text{model discrepancy}} + \underbrace{G_u\bar{G}_u^{-1}\Pi_{u,F}(w_{uF})}_{\text{compensating term}} \tag{13}$$

where $G_u\bar{G}_u^{-1}$ vary with ϕ, $\bar{T}$ and T. Since the aerial manipulator tilts its body toward the pulling direction during the E mode, $G_u\bar{G}_u^{-1}$ differs between the moment of grabbing the wedged object (F $\to$ E) and the moment of extraction (E $\to$ F). Because the value of w_{uF} which effectively compensates for the model discrepancy term in (13) becomes different between the two instances of flight mode change, simply reusing the value of w_{uF} calculated at the instance of F $\to$ E does not help reduce the overshoot in z_u after the object extraction. To solve this problem, during the E mode, we update w_{uF} as if z_u exactly followed $z_{u,d}$ as follows:

$$\begin{aligned} \dot{q}_{uF} &= A_u q_{uF} + B_u z_u, \quad w_{uF} = p_{uF,[1]} - \dot{q}_{uF,[2]}, \\ \dot{p}_{uF} &= A_u p_{uF} + B_u(\ddot{z}_{u,d} + (1-\sigma_u)\Pi_{u,F}(w_{uF})), \end{aligned} \tag{14}$$

where $-\sigma_u\Pi_{u,F}(w_{uF})$ is added for the purpose of performance enhancement with an extremely small positive parameter $\sigma_u \ll 1$.

IEEE Transactions on Automation Science and Engineering (T-ASE) paper, presented at ICRA 2024, Yokohama, Japan.

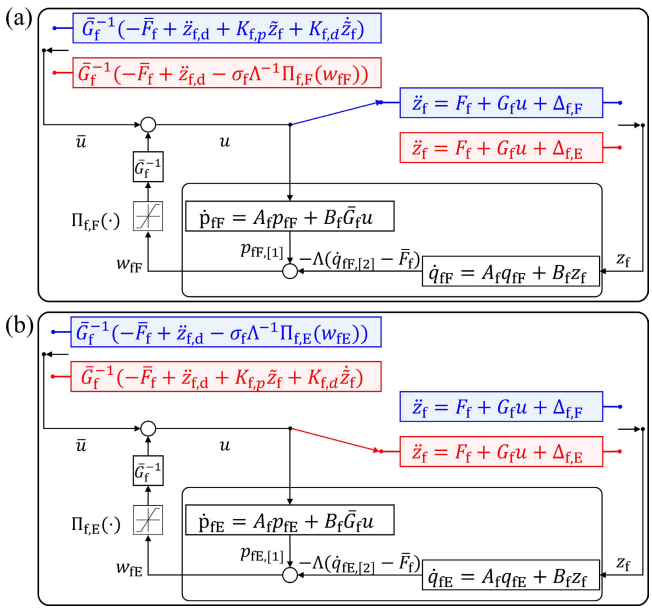

Fig. 4. Update laws for the fully actuated subsystem's inner-DOB variables (a) (p_{fF}, q_{fF}) and (b) (p_{fE}, q_{fE}). Blue and red shaded regions are activated during the F and E modes, respectively.

2) Object-Extracting (E) Mode: With $\bar{\Phi}_d$ calculated in (11), the DOB-based control is formulated as follows:

$$\begin{aligned} \dot{q}_{uE} &= A_u q_{uE} + B_u z_u, \quad \dot{p}_{uE} = A_u p_{uE} + B_u \bar{G}_u \Phi_d, \\ w_{uE} &= p_{uE,[1]} - \dot{q}_{uE,[2]}, \quad \Phi_d = \bar{\Phi}_d + \bar{G}_u^{-1}\Pi_{u,E}(w_{uE}). \end{aligned} \tag{15}$$

As in (14), we update w_{uE} during the F mode as follows:

$$\begin{aligned} \dot{q}_{uE} &= A_u q_{uE} + B_u z_u, \quad w_{uE} = p_{uE,[1]} - \dot{q}_{uE,[2]}, \\ \dot{p}_{uE} &= A_u p_{uE} + B_u(\ddot{z}_{u,d} + (1-\sigma_u)\Pi_{u,E}(w_{uE})). \end{aligned} \tag{16}$$

B. Fully Actuated Subsystem

For each flight mode, u is calculated by the DOB-based control law presented in [21]. As in the underactuated subsystem, we also use different inner variables for each flight mode's DOB: q_{fF}, $p_{fF} \in \mathbb{R}^8$ for the F mode and q_{fE}, $p_{fE} \in \mathbb{R}^8$ for the E mode. Also, to avoid the undesirable peaking in u, we use the saturation functions $\Pi_{f,F}(\cdot)$ and $\Pi_{f,E}(\cdot)$ defined as follows:

- $\Pi_{f,\mu}(\cdot)$: $\mathbb{R}^4 \Rightarrow \mathbb{R}^4$ is a globally bounded $\mathcal{C}^1$ function,
- $\Pi_{f,\mu}(w) = w$, $\forall w \in S_{f,\mu} \triangleq \{w \in \mathbb{R}^4 \mid w = \Lambda\bar{G}_f G_f^{-1}(\bar{F}_f - F_f + (\bar{G}_f - G_f)\bar{u} - \Delta_{f,\mu})\}$,
- $\|\partial\Pi_{f,\mu}(w)/\partial w\| \le 1$.

where $\Lambda \triangleq \text{blockdiag}\{\bar{m}_B, \sqrt{\bar{J}_m} I_3\}$ with the minimum diagonal element of $\bar{J}_B$, $\bar{J}_m$, and $\mu \in \{F, E\}$.

Structures of the following sections will be the same as in the underactuated subsystem.

1) Free-Flight (F) Mode: To make the nominal model (9) asymptotically stable, we set $\bar{u}$ as a PD control

$$\bar{u} = \bar{G}_f^{-1}(-\bar{F}_f + \ddot{z}_{f,d} + K_{f,p}\tilde{z}_f + K_{f,d}\dot{\tilde{z}}_f) \tag{17}$$

where $\tilde{z}_f \triangleq z_{f,d} - z_f$. With $\bar{u}$ defined in (17), to compensate for the model discrepancy between the actual model (3) and the nominal model (9), the DOB-based control law is designed as follows:

$$\begin{aligned} \dot{q}_{fF} &= A_f q_{fF} + B_f z_f, \quad w_{fF} = p_{fF,[1]} - \Lambda(\dot{q}_{fF,[2]} - \bar{F}_f), \\ \dot{p}_{fF} &= A_f p_{fF} + B_f \Lambda \bar{G}_f u, \quad u = \bar{u} + (\Lambda\bar{G}_f)^{-1}\Pi_{f,F}(w_{fF}), \end{aligned} \tag{18}$$

where q_{fF}, $p_{fF} \in \mathbb{R}^8$,

$$A_f \triangleq I_4 \otimes \begin{bmatrix} 0 & 1 \\ -\dfrac{a_{f0}}{\epsilon_f^2} & -\dfrac{a_{f1}}{\epsilon_f} \end{bmatrix}, \quad B_f \triangleq I_4 \otimes [0 \quad a_{f1}/\epsilon_f^2]^\top$$

with positive parameters a_{f0}, a_{f1} and ϵ_f which satisfy $a_{f0}^2/a_{f1} < \frac{1}{2}$ and $\epsilon_f \ll 1$.

If we substitute u in (18) for (3), the dynamic equation is rearranged as follows:

$$\begin{aligned} \ddot{z}_f = \underbrace{\bar{F}_f + \bar{G}_f\bar{u}}_{\text{nominal part}} + \underbrace{(F_f - \bar{F}_f) + (G_f - \bar{G}_f)\bar{u} + \Delta_{f,F}}_{\text{model discrepancy}} \\ + \underbrace{G_f\bar{G}_f^{-1}\Lambda^{-1}\Pi_{f,F}(w_{fF})}_{\text{compensating term}}. \end{aligned} \tag{19}$$

Since $G_f\bar{G}_f^{-1}$ also changes between the moment of object-grabbing (F $\rightarrow$ E) and the moment of object-extraction (E $\rightarrow$ F) owing to the tilting motion of the aerial manipulator during the E mode, the value of w_{fF} suitable for the compensation of the model uncertainty in (19) changes during that period. Therefore, similar to w_{uF}, there needs an update law for w_{fF} during that period. To this end, we update w_{fF} as if z_f exactly followed $z_{f,d}$ during the E mode as follows:

$$\begin{aligned} \dot{q}_{fF} &= A_f q_{fF} + B_f z_f, \quad w_{fF} = p_{fF,[1]} - \Lambda(\dot{q}_{fF,[2]} - \bar{F}_f), \\ \dot{p}_{fF} &= A_f p_{fF} + B_f(\Lambda(-\bar{F}_f + \ddot{z}_{f,d}) + (1-\sigma_f)\Pi_{f,F}(w_{fF})) \end{aligned} \tag{20}$$

where $\sigma_f \ll 1$ is an extremely small positive parameter.

2) Object-Extracting (E) Mode: With $\bar{u}$ calculated in (17), the DOB-based control law is formulated as follows:

$$\begin{aligned} \dot{q}_{fE} &= A_f q_{fE} + B_f z_f, \quad w_{fE} = p_{fE,[1]} - \Lambda(\dot{q}_{fE,[2]} - \bar{F}_f), \\ \dot{p}_{fE} &= A_f p_{fE} + B_f \Lambda \bar{G}_f u, \quad u = \bar{u} + (\Lambda\bar{G}_f)^{-1}\Pi_{f,E}(w_{fE}). \end{aligned} \tag{21}$$

As in (20), q_{fE} and p_{fE} are updated during the F mode as follows:

$$\begin{aligned} \dot{q}_{fE} &= A_f q_{fE} + B_f z_f, \quad w_{fE} = p_{fE,[1]} - \Lambda(\dot{q}_{fE,[2]} - \bar{F}_f), \\ \dot{p}_{fE} &= A_f p_{fE} + B_f(\Lambda(-\bar{F}_f + \ddot{z}_{f,d}) + (1-\sigma_f)\Pi_{f,E}(w_{fE})). \end{aligned} \tag{22}$$

IV. Stability and Performance Analysis

This section presents the stability analysis and the theoretical description on the enhancement of the transient performance after the object extraction. First, we begin with each flight mode and then the transient part between two modes.

IEEE Transactions on Automation Science and Engineering (T-ASE) paper, presented at ICRA 2024, Yokohama, Japan.

A. Stability Analysis

1) Stability Conditions for Each Flight Mode: Based on [7], stability conditions for the aerial manipulator's underactuated subsystem is presented in Proposition 1.

Proposition 1: For each flight mode $\mu \in \{F, E\}$, *let* $(\bar{z}_u(t), \dot{\bar{z}}_u(t))$ *and* $(z_u(t), \dot{z}_u(t))$ *be the solutions of the nominal and actual models of the underactuated subsystem, respectively. With the initial conditions* $\bar{z}_u(0) = z_u(0)$, $\dot{\bar{z}}_u(0) = \dot{z}_u(0)$, $\bar{\Phi}_d(0) = \Phi_d(0)$ *and* $(\bar{z}_u(0), \dot{\bar{z}}_u(0), \bar{\Phi}_d(0), p_{u\mu}(0), q_{u\mu}(0)) \in \bar{\mathcal{S}}_{u,c}$ *where* $\bar{\mathcal{S}}_{u,c}$ *is a compact set, if we assume that* T, $\Delta_{u,\mu}$ *and their time-derivatives* $\dot{T}$, $\dot{\Delta}_{u,\mu}$ *are bounded, then there exists* ϵ_u^* *such that* $[z_u(t)\ \dot{z}_u(t)\ \Phi_d(t)]^\top$ *is uniformly ultimately bounded (UUB) to* $[\bar{z}_u(t)\ \dot{\bar{z}}_u(t)\ \bar{\Phi}_d(t)]^\top$ *for* $0 < \epsilon_u \le \epsilon_u^*$.

Proof: Refer to [7, Theorem 1]. □

Also, as introduced in [21], the stability condition for the aerial manipulator's fully actuated subsystem is described in Proposition 2.

Proposition 2: For each flight mode $\mu \in \{F, E\}$, *let* $(\bar{z}_f(t), \dot{\bar{z}}_f(t))$ *and* $(z_f(t), \dot{z}_f(t))$ *be the solutions of the nominal and actual models of the fully actuated subsystem, respectively. With the initial conditions* $\bar{z}_f(0) = z_f(0)$, $\dot{\bar{z}}_f(0) = \dot{z}_f(0)$, $\bar{u}(0) = u(0)$, $(\bar{z}_u(0), \bar{z}_f(0)), \bar{u}(t), p_{f\mu}(0), q_{f\mu}(0)) \in \bar{\mathcal{S}}_{f,c}$ *where* $\bar{\mathcal{S}}_{f,c}$ *is a compact set, if we assume that* F_f, $\bar{F}_f$, G_f, $\bar{G}_f$ *and* $\Delta_{f,\mu}$ *are* $\mathcal{C}^2$ *functions and bounded in a compact set, then there exists* ϵ_f^* *such that* $[z_f(t)\ u(t)]^\top$ *is UUB to* $[\bar{z}_f(t)\ \bar{u}(t)]^\top$ *for* $0 < \epsilon_f \le \epsilon_f^*$.

Proof: Refer to [21, Theorem 1]. □

According to [7] and [21], the stability conditions for both subsystems are satisfied during the F mode. Thus, there only needs an analysis on the stability during the E mode. From (4), it is proven that $J_{ee}(\chi)$ and F_{ee} are bounded since $\dot{u}$, $\ddot{p}_{Bee}$ and ω_B^B are bounded. Then, since $\Delta_{\mathrm{u,E}} = \Delta_{\mathrm{u,F}} + \frac{1}{m_t}[I_2\ 0_{24}]J_{ee}^\top F_{ee}$, $\Delta_{\mathrm{u,E}}$ and its time-derivative $\dot{\Delta}_{\mathrm{u,E}}$ are also bounded. Thus, the E mode's underactuated subsystem also satisfies the stability conditions stated in Proposition 1. Likewise, since $\Delta_{\mathrm{f,E}} = \Delta_{\mathrm{f,F}} + \frac{1}{m_t}[0_{42}\ I_4]J_{ee}^\top F_{ee}$, $\Delta_{\mathrm{f,E}}$ is a $\mathcal{C}^2$ function and bounded so that the E mode's fully actuated subsystem satisfies the stability conditions introduced in Proposition 2. Therefore, an aerial manipulator under the control laws (15) and (21) also maintains its stability during the E mode.

2) Stability During the Flight Mode Transition: According to [6], stable flight mode transition is guaranteed with continuous $z_{\mathrm{u},d}(t)$, $\dot{z}_{\mathrm{u},d}(t)$, $z_{\mathrm{f},d}(t)$ and $\dot{z}_{\mathrm{f},d}(t)$ while conducting a plug-pulling task. Since the dynamic equation of the plug-pulling aerial manipulator is the same as (4), the stable transition between (1) and (4) is also guaranteed.

B. Analysis on the Transient Performance After the Flight Mode Transition From E to F Mode

1) Meanings of w_{uF} *and* w_{fF}*:* For the underactuated subsystem of the F mode, if we substitute the quasi-static value of w_{uF}, $w_{\mathrm{uF}}^* \triangleq \bar{G}_{\mathrm{u}} G_{\mathrm{u}}^{-1}((\bar{G}_{\mathrm{u}} - G_{\mathrm{u}})\bar{\Phi}_d - \Delta_{\mathrm{u,F}})$, for the rearranged dynamic equation (13), the nominal model (8) is obtained.

Similarly, the rearranged dynamic equation of the fully actuated subsystem of the F mode (19) also approaches its nominal model (9) as w_{fF} reaches its quasi-static value $w_{\mathrm{fF}}^* = \Lambda \bar{G}_{\mathrm{f}} G_{\mathrm{f}}^{-1}(\bar{F}_{\mathrm{f}} - F_{\mathrm{f}} + (\bar{G}_{\mathrm{f}} - G_{\mathrm{f}})\bar{u} - \Delta_{\mathrm{f,F}})$.

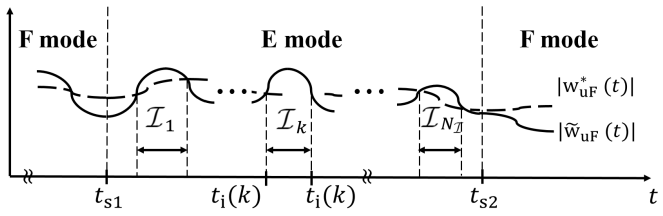

Fig. 5. Behavior of $|\tilde{w}_{\mathrm{uF}}(t)|$ during the E mode.

According to [7, Lemma3] and [21, Lemma 3], w_{uF} and w_{fF} exponentially converge to w_{uF}^* and w_{fF}^*, respectively, with $\epsilon_{\mathrm{u}}, \epsilon_{\mathrm{f}} \to 0$ during the F mode. Therefore, $|\tilde{w}_{\mathrm{uF}}| \triangleq |w_{\mathrm{uF}} - w_{\mathrm{uF}}^*|$ and $|\tilde{w}_{\mathrm{fF}}| \triangleq |w_{\mathrm{fF}} - w_{\mathrm{fF}}^*|$ are sufficiently reduced until the aerial manipulator grabs the wedged object using the DOB-based controller of the F mode.

Note: In **Theorem 1**, we show that $|\tilde{w}_{\mathrm{uF}}(t)|$ maintains its reduced value during the E mode under the update law (14) as shown in Figure 5. Since the analysis on $\tilde{w}_{\mathrm{fF}}$ is similar to that on $\tilde{w}_{\mathrm{uF}}$, we only show the detailed analysis on the behavior of $\tilde{w}_{\mathrm{uF}}$.

2) Analysis on the Behavior of $\tilde{w}_{uF}$ *During the E Mode:* In Figure 5, t_{s1} and t_{s2} represent the first and second mode switching time instances, respectively. Also, we let $\mathcal{I}(k) \triangleq [t_{\mathrm{i}}(k), t_{\mathrm{f}}(k)] \subset [t_{\mathrm{s1}}, t_{\mathrm{s2}}]$ $(k = 1, 2, \cdots, N_\mathcal{I})$ denote the k^{th} time interval which satisfies $|w_{\mathrm{uF}}^*(t)| < |\tilde{w}_{\mathrm{uF}}(t)|$.

We prove that $|\tilde{w}_{\mathrm{uF}}|$ becomes bounded in a certain value $\forall t \in [t_{\mathrm{s1}}\ t_{\mathrm{s2}}]$ during the E mode with (14).

Theorem 1: If p_{uF} *and* q_{uF} *are updated with (14), for* $k = 1, 2, \cdots, N_\mathcal{I}$, *there exist a class* $\mathcal{KL}$ *function* $\beta(\cdot,\cdot)$ *and a class* $\mathcal{K}$ *function* $\gamma(\cdot)$ *such that*

$$|\tilde{w}_{uF}(t)| \le \begin{cases} \beta(|\tilde{w}_{uF}(t_i(k))|, \dfrac{t - t_i(k)}{\epsilon_u}) + \gamma\Big(\sup\limits_{\tau \in \mathcal{I}(k)} |\nu(\tau)|\Big), \\ \qquad\qquad\qquad\qquad \forall t \in \mathcal{I}(k) \\ |w_{uF}^*(t)|, \quad \forall t \in [t_{s1}, t_{s2}] \backslash (\mathcal{I}(1) \cup \cdots \cup \mathcal{I}(N_\mathcal{I})) \end{cases}$$

where $\nu \triangleq -\epsilon_u B_1 \dot{w}_{uF}^* - B_2 a_{u,0} \dddot{\bar{z}}_u$ *with* $B_1 \triangleq I_2 \otimes [1\ 0]^\top$ *and* $B_2 \triangleq I_2 \otimes [0\ 1]^\top$.

Proof: Refer to Appendix. □

V. Experimental Results

This section reports the experimental validation of the proposed controller and the comparison results among the proposed one and two different existing controllers.

A. Experimental Setups

The experimental setup for this research consists of four parts: a quadrotor, a robotic arm, a frame for the plug-socket system, and a plug on/off determination system. The quadrotor was assembled with the off-the-shelf frame DJI S500, four U3-KV700 motors with corresponding ALPHA-40A-LV electronic speed controllers, and 12-inch T-Motor carbon fiber propellers, two Turnigy LiPo batteries for power supplement, and Intel NUC for computing. On Intel NUC, Robot Operating System (ROS) is installed in Ubuntu 18.04, and the position controller for the quadrotor, joint angle controller for the

IEEE Transactions on Automation Science and Engineering (T-ASE) paper, presented at ICRA 2024, Yokohama, Japan.

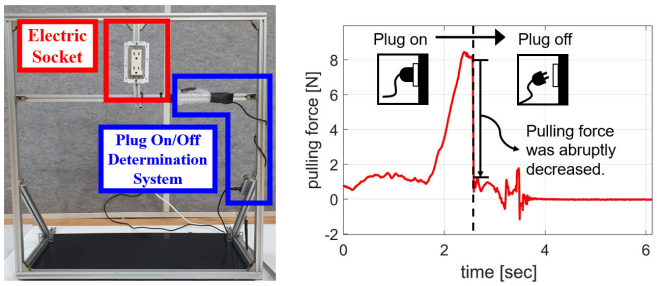

Fig. 6. (a) Plug-socket system with a plug on/off determination system. (b) History of the pulling force exerted on the end-effector.

TABLE I

PARAMETER SETTING FOR THE CONTROL OF UNDERACTUATED SUBSYSTEM

$\bar{m}_B$		$K_{\mathrm{u}P}$	$K_{\mathrm{u}D}$
2.50 kg		$\mathrm{diag}\{1.00, 1.00\}$	$\mathrm{diag}\{2.00, 2.00\}$
$a_{\mathrm{u}0}$	$a_{\mathrm{u}1}$	ϵ_{u}	σ_{u}
1.00	2.00	0.100	0.0500

TABLE II

PARAMETER SETTING FOR THE CONTROL OF FULLY ACTUATED SUBSYSTEM

J_B		$K_{\mathrm{f}P}$	
$\mathrm{diag}\{0.200, 0.200, 0.100\}$ kgm^2		$\mathrm{diag}\{9.00, 0.00280, 0.0280, 0.700\}$	
		$K_{\mathrm{f}D}$	
		$\mathrm{diag}\{6.00, 0.0189, 0.0560, 0.100\}$	
$a_{\mathrm{f}0}$	$a_{\mathrm{f}1}$	ϵ_{f}	σ_{f}
1.00	2.00	0.100	0.0500

robotic arm, and the navigation algorithm with Optitrack are executed. The attitude controllers are implemented in Pixhawk 4 which is connected to the Intel NUC. The robotic arm is comprised of ROBOTIS dynamixel XH540 and XM430 servo motors, and the built-in software makes their angles track their desired values. A stand for a 110 V socket is firmly attached to a black plastic plate as in Figure 6. The plug on/off determination system which publishes the signal indicating whether the plug is separated from the socket or not is comprised of AAEON UP Board and Arduino mini. We use this because sensing the flight mode change is not the main goal of this research.

Additionally, we use the 2-axis force/torque (FT) sensor FUTEK MBA500 to measure the magnitude of the pulling force during the process of plug-pulling by hands. Note that we did not use this FT sensor during the flight experiment.

For the control of the underactuated subsystem, we set the controller parameters as in Table I.

Meanwhile, the saturation function $w_{\mathrm{u},\pi} \triangleq \Pi_{\mathrm{u},\mu}(w)$ is set as:

$$w_{\mathrm{u},\pi,i} = \begin{cases} 5.00, & 5.00 < w_i \\ w_i, & -5.00 \leq w_i \leq 5.00 \\ -5.00, & w_i < -5.00. \end{cases}$$

The controller parameters of the fully actuated subsystem are set as in Table II.

TABLE III

MAXIMUM VALUES OF POSITION DEVIATION AND TILT ANGLE DURING THE TRANSIENT TIME INTERVAL FOR 4 SECONDS FROM THE TIME INSTANCE OF THE PLUG SEPARATION. THE BEST VALUES ARE HIGHLIGHTED IN BOLD

	Maximum value of	
	position deviation [m]	tilt angle [deg]
1) Baseline 1	0.6014	20.39
2) Baseline 2	0.4517	31.50
3) Proposed	**0.3131**	**4.619**

Also, we set the output of the saturation function $w_{\mathrm{f},\pi} \triangleq \Pi_{\mathrm{f},\mu}(w)$ as follows:

$$w_{\mathrm{f},\pi,i} = \begin{cases} 100, & 100 < w_i \\ w_i, & -100 \leq w_i \leq 100 \\ -100, & w_i < -100. \end{cases}$$

Note that the PixHawk 4's attitude controller generates the normalized torque $\tau_{B,\mathrm{nom}} \triangleq [\tau_{B,1}/\tau_{B,x,\max} \tau_{B,2}/\tau_{B,y,\max} \tau_{B,3}/\tau_{B,z,\max}]^\top$ based on the above parameters instead of the actual torque τ_B. Here, we let $\tau_{B,x,\max}$, $\tau_{B,y,\max}$ and $\tau_{B,z,\max}$ denote the maximum torques w.r.t. x, y and z axes of the multirotor frame, respectively.

B. Scenario

First, the end-effector of the aerial manipulator approaches the plug. Then, the end-effector grabs and pulls the plug by setting the desired position to a position 30 cm away from the current position in the pulling direction and converting the control mode to the E mode. After the plug separation, the plug on/off determination system sends a plug-off signal to the onboard computer, and the control mode returns to the F mode. Finally, the aerial manipulator maintains its hovering state.

To validate the performance improvement by our controller, we conduct the plug-pulling experiment using the three controllers: 1) DOB-based controller presented in [7] and [21] without flight mode separation, 2) arbitrary initialization of the DOBs' inner variables when the flight mode is changed (initialize with zero vectors in this case) and 3) proposed hybrid controller.

C. Results

Figure 7a presents the measured value of χ, the joint angle & current of a servo motor mounted on the multirotor (θ_1 & i_1), and the PWM inputs to each motor when the DOB-based controller introduced in [7] and [21] without flight mode separation is employed. As observed in the measured value of p after the plug separation, the quadrotor was not able to maintain the hovering state. Also, from the PWM results, we can notice that those values significantly oscillate after the flight mode is changed from E to F. This result shows that using the single mode controller can result in a large overshoot in χ or destabilization. Indeed, the attached video shows that the aerial manipulator using this control method crashes to the ground after the plug separation.

IEEE Transactions on Automation Science and Engineering (T-ASE) paper, presented at ICRA 2024, Yokohama, Japan.

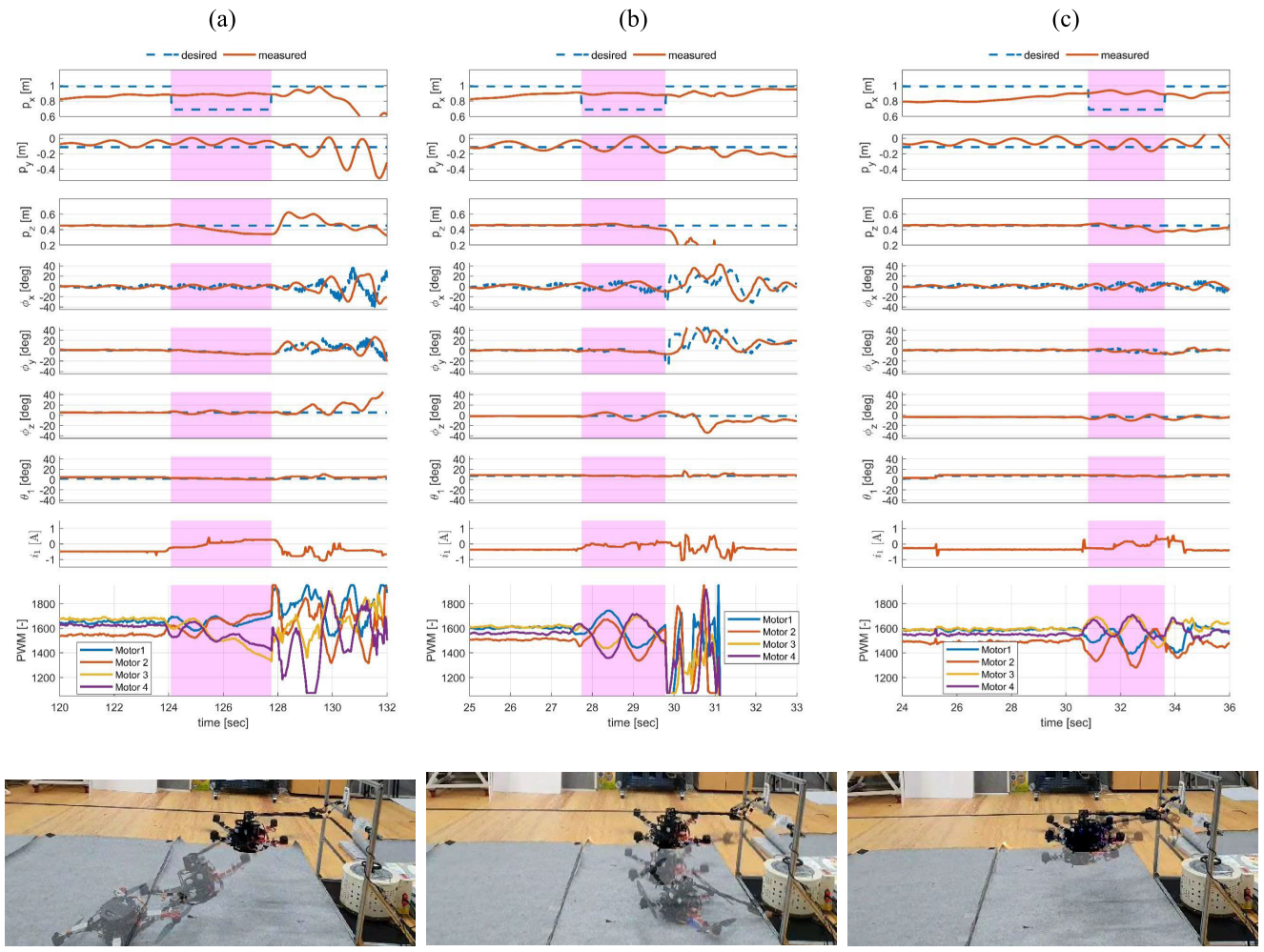

Fig. 7. History of the quadrotor states ($\chi = [p^\top \ \phi^\top]^\top$), joint angle & current of a servo motor mounted on the quadrotor (θ_1 & i_1), PWM inputs into each motor, and snapshots. The white region and the magenta region express the F mode and the E mode, respectively. For the values of states, joint angle, and joint current, the dashed blue lines show the desired values of the states, and the red lines represent the measured values of the states. For the values of motor PWM, blue, red, yellow, and purple lines represent the PWM inputs of the first, second, third, and fourth motors, respectively. The numbers of the motors are introduced in [24]. (a) (Baseline 1) DOB-based controller without flight mode separation, (b) (Baseline 2) initializing the DOBs' inner variables with zero vectors when the flight mode is changed, (c) **(Proposed)** hybrid controller enhancing transient performance.

In Figure 7b, p_{uF}, q_{uF}, p_{fF} and q_{fF} are reset to zero matrices when the flight mode is changed from E to F mode. From the result of p_z, we can observe that the quadrotor suddenly descends to the ground. Furthermore, we can observe that the PWM values of all motors suddenly descend to their lowest values after the plug separation. This phenomenon occurs because the initial value of w_{fF} is far from the value which sufficiently compensates for the model discrepancy between the actual model of the fully actuated subsystem of the F mode (3) and its nominal model (9). As can be seen in the attached video, the aerial manipulator cannot recover its hovering state after the plug separation.

Compared with Figures. 7a and 7b, the result using the proposed controller in Figure 7c shows satisfactory performance after the object extraction. At the moment of the flight mode transition (around 34 s), none of χ shows significant overshoot. Additionally, all motors' PWM values show more stable behavior than those of the other experiments. From this result, it is verified that w_{uF} and w_{fF} updated along with (12), (18), (14) and (20) successfully preserve the reduced values of $\tilde{w}_{\mathrm{uF}}$ and $\tilde{w}_{\mathrm{fF}}$, respectively. Also, we can see that the aerial manipulator satisfactorily maintains its hovering state after the plug separation in the attached video.

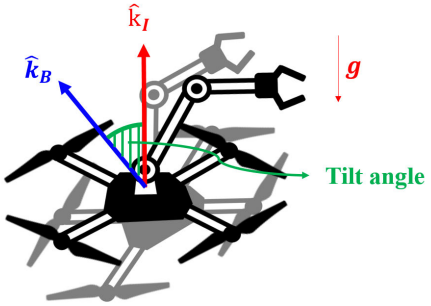

Fig. 8. Graphical description of the tilt angle between the z-axis of the inertial frame ($\hat{k}_I$) and the z-axis of the multirotor frame ($\hat{k}_B$).

To quantitatively compare the transient performances of the three controllers, we observe the maximum values of the position deviation $|p_{b,d} - p_b|$ and the tilt angle explained in Figure 8 during the transient time interval $[t_{s2}, t_{s2} + 4]$ sec where t_{s2} represents the time instance of plug separation. As observed in Table III, the result using the proposed

IEEE Transactions on Automation Science and Engineering (T-ASE) paper, presented at ICRA 2024, Yokohama, Japan.

controller shows the best performance both in the position deviation and tilt angle.

After the flight experiment, we manually pulled the plug to obtain the history of pulling force exerted on the end-effector during the plug-pulling. As shown in Figure 6b, the pulling force abruptly decreased from 8 N to 0 N due to the plug separation around 2.5 seconds. Since the weight of the aerial manipulator is around 30 N and the maximum thrust of 4 motors is around 60 N, 8 N is a relatively large force to generate. Therefore, since the change from 8 N to 0 N can be interpreted as a large decrease, our experimental setting is appropriate to test the abrupt change in dynamics.

VI. Conclusion

This paper presents a hybrid controller enhancing transient performance for an aerial manipulator extracting an object wedged in a static structure. To analyze the dynamic characteristics, the dynamic equations for two flight modes, i.e., free-flight and object-extracting, the rule of state jumps and the corresponding nominal models are derived. Also, we design each flight mode's DOB-based control laws and strategies to enhance the transient performance after the flight mode transition. Then, the stability of the aerial manipulator is proven and the capability to reduce the overshoot in the state variable after the object extraction is demonstrated. To validate the satisfactory performance of our controller, we conduct plug-pulling experiments using the proposed controller and two different existing controllers. As a result, it is shown that our controller enables the aerial manipulator to maintain its stability after the flight mode transition and shows the best performance in overshoot minimization among three controllers. For future works, we may design a controller for an aerial manipulator experiencing a discontinuous state jump during the flight mode transition. Also, we may devise a control strategy which deals with more than three flight modes.

Appendix

First, we define the augmented variable $\eta_{\mathrm{uF}} \in \mathbb{R}^4$ as follows:

$$\begin{aligned}\eta_{\mathrm{uF}} &\triangleq B_1 w_{\mathrm{uF}} + \epsilon_{\mathrm{u}} B_2 \dot{w}_{\mathrm{uF}} \\ &= B_1(p_{\mathrm{uF},[1]} - \dot{q}_{\mathrm{uF},[2]}) + \epsilon_{\mathrm{u}} B_2(\dot{p}_{\mathrm{uF},[1]} - \ddot{q}_{\mathrm{uF},[2]}) \end{aligned} \tag{23}$$

By differentiating η_{uF} with respect to time

$$\begin{aligned}\dot{\eta}_{\mathrm{uF}} &= B_1 \dot{w}_{\mathrm{uF}} + \epsilon_{\mathrm{u}} B_2(\ddot{p}_{\mathrm{uF},[1]} - \dddot{q}_{\mathrm{uF},[2]}) \\ &= B_1 \dot{w}_{\mathrm{uF}} + \epsilon_{\mathrm{u}} B_2\Big(\frac{a_{\mathrm{u},0}}{\epsilon_{\mathrm{u}}^2}(\dddot{\tilde{z}}_{\mathrm{u}} + (1-\sigma_{\mathrm{u}})\Pi_{\mathrm{u,F}}(w_{\mathrm{uF}})) \\ &\quad - \frac{a_{\mathrm{u},0}}{\epsilon_{\mathrm{u}}^2}\big(p_{\mathrm{uF},[1]} - \dot{q}_{\mathrm{uF},[2]} - \frac{a_{\mathrm{u},1}}{\epsilon_{\mathrm{u}}}(\dot{p}_{\mathrm{uF},[1]} - \ddot{q}_{\mathrm{uF},[2]})\big) \\ &= B_1 \dot{w}_{\mathrm{uF}} + \epsilon_{\mathrm{u}} B_2 \\ &\quad \times \Big(\frac{a_{\mathrm{u},0}[\dddot{\tilde{z}}_{\mathrm{u}} + (1-\sigma_{\mathrm{u}})\Pi_{\mathrm{u,F}}(w_{\mathrm{uF}}) - \eta_{\mathrm{u},[1]}] + a_{\mathrm{u},1}\eta_{\mathrm{uF},[2]}}{\epsilon_{\mathrm{u}}^2}\Big),\end{aligned}$$

then substituting $\eta_{\mathrm{uF},[1]} = B_1 \eta_{\mathrm{uF}} = w_{\mathrm{uF}}$, we obtain

$$\epsilon_{\mathrm{u}} \dot{\eta}_{\mathrm{uF}} = A_{\mathrm{u},\tilde{\eta}} \eta_{\mathrm{uF}} + B_2 a_{\mathrm{u},0}[\dddot{\tilde{z}}_{\mathrm{u}} + (1-\sigma_{\mathrm{u}})\Pi_{\mathrm{u,F}}(w_{\mathrm{uF}}) - w_{\mathrm{uF}}] \tag{24}$$

where $A_{\mathrm{u},\tilde{\eta}} \triangleq I_2 \otimes \begin{bmatrix} 0 & 1 \\ 0 & -a_{\mathrm{u},1} \end{bmatrix}$.

Letting $\tilde{\eta}_{\mathrm{uF}}$ denote $B_1 \tilde{w}^{\mathrm{uF}} + B_2 \eta_{\mathrm{uF},[2]}$, (24) is rearranged as follows:

$$\epsilon_{\mathrm{u}} \dot{\tilde{\eta}}_{\mathrm{u}} = A_{\mathrm{u},\tilde{\eta}} \tilde{\eta}_{\mathrm{u}} + B_2 a_{\mathrm{u},0}(-\psi(\tilde{w}_{\mathrm{uF}})) + \nu \tag{25}$$

where $\psi(\tilde{w}_{\mathrm{uF}}) \triangleq -(1-\sigma_{\mathrm{u}})\Pi_{\mathrm{u,F}}(w_{\mathrm{uF}}) + w_{\mathrm{u}}^* + \tilde{w}_{\mathrm{u}}$.

By setting ν to 0_{21}, the unforced system of (25) with the output $\tilde{w}_{\mathrm{uF}}$ is rearranged as follows:

$$\tilde{\eta}_{\mathrm{uF}}{}' = A_{\mathrm{u},\tilde{\eta}} \tilde{\eta}_{\mathrm{u}} + B_2 a_{\mathrm{u},0}(-\psi(\tilde{w}_{\mathrm{uF}})), \quad \tilde{w}_{\mathrm{uF}} = B_1 \tilde{\eta}_{\mathrm{uF}} \tag{26}$$

where $(\cdot)' \triangleq \epsilon_{\mathrm{u}} \frac{d(\cdot)}{dt}$. For all $t \in \mathcal{I}(1) \cup \cdots \cup \mathcal{I}(N_{\mathcal{I}})$, since $|w_{\mathrm{uF}}^*| < |\tilde{w}_{\mathrm{uF}}|$, there exists a positive number $\kappa \in (0, \sigma_{\mathrm{u}})$ which satisfies the following inequality:

$$\sigma_{\mathrm{u}} |w_{\mathrm{uF}}^*(t)| \le (\sigma_{\mathrm{u}} - \kappa)|\tilde{w}_{\mathrm{uF}}(t)|. \tag{27}$$

Then, since $\Pi_{\mathrm{u,F}}(w_{\mathrm{uF}}^*) = w_{\mathrm{uF}}^*$, the following inequality also holds:

$$\begin{aligned}&|\psi(\tilde{w}_{\mathrm{uF}}) - \tilde{w}_{\mathrm{uF}}| \\ &\quad = |(1-\sigma_{\mathrm{u}})(\Pi_{\mathrm{u,F}}(w_{\mathrm{uF}}) - \Pi_{\mathrm{u,F}}(w_{\mathrm{uF}}^*)) - \sigma_{\mathrm{u}}\Pi_{\mathrm{u,F}}(w_{\mathrm{uF}}^*)| \\ &\quad \le (1-\sigma_{\mathrm{u}})|(\Pi_{\mathrm{u,F}}(w_{\mathrm{uF}}) - \Pi_{\mathrm{u,F}}(w_{\mathrm{uF}}^*))| + \sigma_{\mathrm{u}}|\Pi_{\mathrm{u,F}}(w_{\mathrm{uF}}^*)| \\ &\quad \le (1-\kappa)|\tilde{w}_{\mathrm{uF}}|.\end{aligned}$$

Hence, the sector condition $\psi(\tilde{w}_{\mathrm{uF}}) \in [(1-\kappa)I_2, (1+\kappa)I_2]$ holds $\forall t \in \mathcal{I}(k)$ for $k = 1, 2, \cdots, N_{\mathcal{I}}$.

From [25, Theorem 7.1], we prove that the unforced system (26) is strictly positive real since $\psi(\tilde{\eta}_{\mathrm{uF},[1]}) = \psi(\tilde{w}_{\mathrm{uF}}) \in [(1-\kappa)I_2, (1+\kappa)I_2]$ and $a_{\mathrm{u},0}^2/a_{\mathrm{u},1} < \frac{1}{2}$. Therefore, there exists a positive definite matrix $P_{\tilde{\eta}} = P_{\tilde{\eta}}^\top$ and a positive number ε such that

$$\begin{aligned}\alpha_1(|\tilde{\eta}_{\mathrm{uF}}|) \le V_{\tilde{\eta}} \le \alpha_2(|\tilde{\eta}_{\mathrm{uF}}|) \\ \frac{\partial V_{\tilde{\eta}}}{\partial \tilde{\eta}_{\mathrm{uF}}}(A_{\mathrm{u},\tilde{\eta}}\tilde{\eta}_{\mathrm{uF}} + B_2 a_{\mathrm{u},0}(-\psi(\tilde{w}_{\mathrm{uF}}))) \le -\alpha_3(|\tilde{\eta}_{\mathrm{uF}}|)\end{aligned} \tag{28}$$

where $V_{\tilde{\eta}} \triangleq \frac{1}{2}\tilde{\eta}_{\mathrm{u}}^\top P_{\tilde{\eta}} \tilde{\eta}_{\mathrm{u}}$, $\alpha_1(\cdot) \triangleq \frac{1}{2}\lambda_{min}(P_{\tilde{\eta}})(\cdot)^2$, $\alpha_2(\cdot) \triangleq \frac{1}{2}\lambda_{max}(P_{\tilde{\eta}})(\cdot)^2$ and $\alpha_3(\cdot) \triangleq \frac{1}{2}\varepsilon\lambda_{min}(P_{\tilde{\eta}})(\cdot)^2$. From (25), the upper bound of $V_{\tilde{\eta}}{}'$ is derived as follows:

$$\begin{aligned}V_{\tilde{\eta}}{}' &\le -\alpha_3(|\tilde{\eta}_{\mathrm{uF}}|) + \tilde{\eta}_{\mathrm{uF}}^\top P_{\tilde{\eta}} \nu \le -(1-\rho)\alpha_3(|\tilde{\eta}_{\mathrm{uF}}|) \\ &\quad - \rho\alpha_3(|\tilde{\eta}_{\mathrm{uF}}|) + r_M \|P_{\tilde{\eta}}\| \sup_{\tau \in \mathcal{I}(k)} |\nu(\tau)|\end{aligned} \tag{29}$$

where r_M is defined as a positive number which satisfies $|\tilde{w}_{\mathrm{uF}}(t)| \le r_M, \forall t \in [t_{\mathrm{s}1}, t_{\mathrm{s}2}]$ with $0 < \rho < 1$.

Since both $|\dddot{\tilde{z}}_{\mathrm{u}}|$ and ϵ_{u} are bounded, there exists a sufficiently small positive number r_ν such that $|\sup_{\tau \in \mathcal{I}(k)} \nu(\tau)| \le r_\nu$. Thus, a positive number $r_m \triangleq \alpha_1^{-1}\Big(r_M \|P_{\tilde{\eta}}\| \sup_{\tau \in \mathcal{I}(k)} |\nu(\tau)|/\rho\Big)$ satisfies $r_m < \alpha_2^{-1}(\alpha_1(r_M))$ and makes $V_{\tilde{\eta}}{}' \le -(1-\rho)\alpha_3(|\tilde{\eta}_{\mathrm{uF}}|)$, $\forall |\tilde{\eta}_{\mathrm{uF}}| \ge r_m$.

According to [25, Theorem 4.18], since $V_{\tilde{\eta}}{}' \le -\alpha_4(|\tilde{\eta}_{\mathrm{uF}}|)$ holds for the class $\mathcal{K}$ function $\alpha_4(\cdot) \triangleq (1-\rho)\alpha_3(\cdot)$, there exists a $\mathcal{KL}$ function $\beta'(\cdot,\cdot)$ such that

$$\begin{aligned}|\tilde{\eta}_{\mathrm{uF}}(t)| \le \beta'\big(|\tilde{\eta}_{\mathrm{uF}}(t_{\mathrm{i}}(k))|, \frac{t - t_{\mathrm{i}}(k)}{\epsilon_{\mathrm{u}}}\big) \\ + \gamma\Big(\sup_{t \in \mathcal{I}(k)} |\nu(t)|\Big), \quad \forall t \in \mathcal{I}(k)\end{aligned}$$

IEEE Transactions on Automation Science and Engineering (T-ASE) paper, presented at ICRA 2024, Yokohama, Japan.

Also, since $|\dot{\tilde{\eta}}_{\mathrm{uF},[2]}|$ is bounded, there exists a $\mathcal{KL}$ function $\beta(\cdot,\cdot)$ such that $\beta'(|\tilde{\eta}_{\mathrm{uF}}(t_{\mathrm{i}}(k))|, \frac{t-t_{\mathrm{i}}(k)}{\epsilon_{\mathrm{u}}}) \leq \beta(|\tilde{w}_{\mathrm{uF}}(t_{\mathrm{i}}(k))|, \frac{t-t_{\mathrm{i}}(k)}{\epsilon_{\mathrm{u}}})$ holds. Thus, for $k = 1, 2, \cdots, N_{\mathcal{I}}$, the following inequality holds:

$$|\tilde{w}_{\mathrm{uF}}(t)| \leq \beta\big(|\tilde{w}_{\mathrm{uF}}(t_{\mathrm{i}}(k))|, \frac{t-t_{\mathrm{i}}(k)}{\epsilon_{\mathrm{u}}}\big) + \gamma\Big(\sup_{\tau\in\mathcal{I}(k)}|\nu(\tau)|\Big),\ \forall t \in \mathcal{I}(k)$$

REFERENCES

[1] M. Orsag, C. Korpela, S. Bogdan, and P. Oh, "Valve turning using a dual-arm aerial manipulator," in *Proc. Int. Conf. Unmanned Aircr. Syst. (ICUAS)*, May 2014, pp. 836–841.

[2] S. Kim, H. Seo, and H. J. Kim, "Operating an unknown drawer using an aerial manipulator," in *Proc. IEEE Int. Conf. Robot. Autom. (ICRA)*, May 2015, pp. 5503–5508.

[3] D. Lee, H. Seo, D. Kim, and H. J. Kim, "Aerial manipulation using model predictive control for opening a hinged door," in *Proc. IEEE Int. Conf. Robot. Autom. (ICRA)*, May 2020, pp. 1237–1242.

[4] Y. Sun, Z. Jing, P. Dong, J. Huang, W. Chen, and H. Leung, "A switchable unmanned aerial manipulator system for window-cleaning robot installation," *IEEE Robot. Autom. Lett.*, vol. 6, no. 2, pp. 3483–3490, Apr. 2021.

[5] J. Delmerico et al., "The current state and future outlook of rescue robotics," *J. Field Robot.*, vol. 36, no. 7, pp. 1171–1191, Oct. 2019.

[6] J. Byun, D. Lee, H. Seo, I. Jang, J. Choi, and H. J. Kim, "Stability and robustness analysis of plug-pulling using an aerial manipulator," in *Proc. IEEE/RSJ Int. Conf. Intell. Robots Syst. (IROS)*, Sep. 2021, pp. 4199–4206.

[7] D. Lee, H. Seo, I. Jang, S. J. Lee, and H. J. Kim, "Aerial manipulator pushing a movable structure using a DOB-based robust controller," *IEEE Robot. Autom. Lett.*, vol. 6, no. 2, pp. 723–730, Apr. 2021.

[8] H. Lee, S. Kim, and H. J. Kim, "Control of an aerial manipulator using on-line parameter estimator for an unknown payload," in *Proc. IEEE Int. Conf. Autom. Sci. Eng. (CASE)*, Aug. 2015, pp. 316–321.

[9] M. Ryll et al., "6D physical interaction with a fully actuated aerial robot," in *Proc. IEEE Int. Conf. Robot. Autom. (ICRA)*, May 2017, pp. 5190–5195.

[10] G. Baraban, M. Sheckells, S. Kim, and M. Kobilarov, "Adaptive parameter estimation for aerial manipulation," in *Proc. Amer. Control Conf. (ACC)*, Jul. 2020, pp. 614–619.

[11] J. Liang, Y. Chen, Y. Wu, Z. Miao, H. Zhang, and Y. Wang, "Adaptive prescribed performance control of unmanned aerial manipulator with disturbances," *IEEE Trans. Autom. Sci. Eng.*, early acces, Jul. 1, 2022, doi: 10.1109/TASE.2022.3186315.

[12] J. Á. Acosta, M. I. Sánchez, and A. Ollero, "Robust control of underactuated aerial manipulators via IDA-PBC," in *Proc. 53rd IEEE Conf. Decis. Control*, Dec. 2014, pp. 673–678.

[13] M. Orsag, C. Korpela, S. Bogdan, and P. Oh, "Lyapunov based model reference adaptive control for aerial manipulation," in *Proc. Int. Conf. Unmanned Aircr. Syst. (ICUAS)*, May 2013, pp. 966–973.

[14] J. L. J. Scholten, M. Fumagalli, S. Stramigioli, and R. Carloni, "Interaction control of an UAV endowed with a manipulator," in *Proc. IEEE Int. Conf. Robot. Autom.*, May 2013, pp. 4910–4915.

[15] A. Praveen, X. Ma, H. Manoj, V. LN. Venkatesh, M. Rastgaar, and R. M. Voyles, "Inspection-on-the-fly using hybrid physical interaction control for aerial manipulators," in *Proc. IEEE/RSJ Int. Conf. Intell. Robots Syst. (IROS)*, Oct. 2020, pp. 1583–1588.

[16] Y. Yu and X. Ding, "On hybrid modeling and control of a multi-propeller multifunction aerial robot with flying-walking locomotion," *Auto. Robots*, vol. 38, no. 3, pp. 225–242, Mar. 2015.

[17] H. Nguyen and K. Alexis, "Forceful aerial manipulation based on an aerial robotic chain: Hybrid modeling and control," *IEEE Robot. Autom. Lett.*, vol. 6, no. 2, pp. 3711–3719, Apr. 2021.

[18] L. Marconi and R. Naldi, "Control of aerial robots: Hybrid force and position feedback for a ducted fan," *IEEE Control Syst.*, vol. 32, no. 4, pp. 43–65, Aug. 2012.

[19] G. Darivianakis, K. Alexis, M. Burri, and R. Siegwart, "Hybrid predictive control for aerial robotic physical interaction towards inspection operations," in *Proc. IEEE Int. Conf. Robot. Autom. (ICRA)*, Jun. 2014, pp. 53–58.

[20] D. Cabecinhas, R. Naldi, C. Silvestre, R. Cunha, and L. Marconi, "Robust landing and sliding maneuver hybrid controller for a quadrotor vehicle," *IEEE Trans. Control Syst. Technol.*, vol. 24, no. 2, pp. 400–412, Mar. 2016.

[21] S. Kim, S. Choi, H. Kim, J. Shin, H. Shim, and H. J. Kim, "Robust control of an equipment-added multirotor using disturbance observer," *IEEE Trans. Control Syst. Technol.*, vol. 26, no. 4, pp. 1524–1531, Jul. 2018.

[22] H. Yang and D. Lee, "Dynamics and control of quadrotor with robotic manipulator," in *Proc. IEEE Int. Conf. Robot. Autom. (ICRA)*, Jun. 2014, pp. 5544–5549.

[23] R. Goebel, R. G. Sanfelice, and A. R. Teel, *Hybrid Dynamical Systems*. Princeton, NJ, USA: Princeton Univ. Press, 2012.

[24] *Airframes Reference*. Accessed: Mar. 9, 2023. [Online]. Available: https://dev.px4.io/master/en/airframes/airframe_reference.html

[25] H. K. Khalil, *Nonlinear Systems*, 3rd ed. Upper Saddle River, NJ, USA: Prentice-Hall, 2002.

Jeonghyun Byun (Graduate Student Member, IEEE) received the B.S. degree in aerospace engineering from Seoul National University, Seoul, South Korea, in 2020, where he is currently pursuing the Ph.D. degree in aerospace engineering with the Department of Aerospace Engineering.

His current research interests include control and planning of aerial robots.

Inkyu Jang (Graduate Student Member, IEEE) received the B.S. degree in mechanical engineering from Seoul National University, Seoul, South Korea, in 2020, where he is currently pursuing the Ph.D. degree in aerospace engineering with the Department of Aerospace Engineering.

His research interests include robust motion planning of mobile robots.

Dongjae Lee (Graduate Student Member, IEEE) received the B.S. and M.S. degrees in mechanical and aerospace engineering from Seoul National University, Seoul, South Korea, in 2018 and 2020, respectively, where he is currently pursuing the Ph.D. degree in aerospace engineering.

His current research interests include the control and planning of robotic systems.

H. Jin Kim (Member, IEEE) received the B.S. degree in mechanical engineering from the Korean Advanced Institute of Technology, Daejeon, South Korea, in 1995, and the M.S. and Ph.D. degrees in mechanical engineering from the University of California at Berkeley, Berkeley, CA, USA, in 1999 and 2001, respectively.

From 2002 to 2004, she was a Post-Doctoral Researcher with the Department of Electrical Engineering and Computer Science, University of California, Berkeley. In 2004, she joined the School of Mechanical and Aerospace Engineering, Seoul National University, Seoul, South Korea, where she is currently a Professor. Her research interests include navigation and motion planning of autonomous robotic systems.